The Journal of Experimental Biology 209, 2409-2419
Published by The Company of Biologists 2006
doi:10.1242/jeb.02257

Hot limpets: predicting body temperature in a conductance-mediated thermal system

Mark W. Denny[1,*] and Christopher D. G. Harley[1,2]

[1]*Hopkins Marine Station of Stanford University, Pacific Grove, CA 93950, USA and* [2]*Department of Zoology, University of British Columbia, Vancouver, BC, V6T 1Z4, Canada*

*Author for correspondence (e-mail: mwdenny@stanford.edu)

Accepted 6 April 2006

Summary

Living at the interface between the marine and terrestrial environments, intertidal organisms may serve as a bellwether for environmental change and a test of our ability to predict its biological consequences. However, current models do not allow us to predict the body temperature of intertidal organisms whose heat budgets are strongly affected by conduction to and from the substratum. Here, we propose a simple heat-budget model of one such animal, the limpet *Lottia gigantea*, and test the model against measurements made in the field. Working solely from easily measured physical and meteorological inputs, the model predicts the daily maximal body temperatures of live limpets within a fraction of a degree, suggesting that it may be a useful tool for exploring the thermal biology of limpets and for predicting effects of climate change. The model can easily be adapted to predict the temperatures of chitons, acorn barnacles, key-hole limpets, and encrusting animals and plants.

Key words: heat-budget model, intertidal zone, thermal limits, limpet, *Lottia gigantean*, heat stress.

Introduction

The intertidal zone of wave-swept rocky shores is among the most physically stressful on earth. When the tide is in, plants and animals are subjected to challenging hydrodynamic forces. When the tide recedes, organisms are exposed to terrestrial conditions in which they may desiccate and reach stressful temperatures. Despite the physical severity of the intertidal environment, the plants and animals of wave-swept shores are abundant, productive and diverse.

This unusual combination of biological diversity in the face of physical adversity has been the impetus for extensive research regarding the physiological capabilities of intertidal organisms and the role physiology plays in ecological interactions among them. Several patterns are now well established. For example, the upper limit to a species' range on the shore is often set by the physical environment (Rafaelli and Hawkins, 1996; Helmuth et al., 2005), and manipulation of environmental conditions has the potential to shift biological zonation patterns (Wethey, 1984; Harley, 2003). Severe physiological stress and subsequent mortality of spatial dominants can be an important agent of disturbance in intertidal assemblages (Tsuchiya, 1983). Finally, by disproportionately affecting certain species within a community, environmental stress can alter the strength and even the sign of interspecific interactions (Leonard, 2000).

Because their survival and performance are strongly tied to the physical environment, intertidal organisms potentially serve as a sensitive bellwether of global climate change. The strength of this abiotic–biotic coupling, along with several decades of intensive physiological and ecological research, make the intertidal zone an excellent model system in which to test our ability to predict the biological consequences of future environmental change, particularly with regards to climatic warming. There are gaps, however, in our armament of predictive tools. Although physiological studies have begun to define the thermal limits of a variety of intertidal plants and animals (e.g. Wolcott, 1973; Newell, 1979; Bell, 1995; Hoffman and Somero, 1996; Davison and Pearson, 1996; Stillman and Somero, 2000; Tomanek, 2002; Dethier et al., 2005), we have a limited capacity to predict when and where organisms reach these limits (Helmuth et al., 2005).

Currently, there are two detailed published models for the thermal behavior of intertidal organisms that allow prediction of body temperature from standard meteorological parameters. Bell constructed heat-budget model for the foliose red alga, *Mastocarpus papillatus* Kützing (Bell, 1995). Conductive transfer of heat between the alga and the rock substratum is negligible. Instead, the temperature of this seaweed is controlled primarily by the interplay of heat coming into the organism from solar radiation and heat being lost by a combination of evaporation and convective transfer to the air. A heat budget model was also constructed for the mussel,

Mytilus californianus Conrad (Helmuth, 1998). Again, the temperature of the organism is controlled primarily by the rate at which heat is absorbed from the sun and the rate at which heat is lost by evaporation and convective transfer to the air. Helmuth's model allows for conductive transfer of heat to and from the rock substratum (controlled by the temperature gradient in the animal rather than in the rock), but because contact area between the mussel and the rock is very small, conduction is seldom an important component of a mussel's overall heat budget. Furthermore, Helumth's model requires that rock temperature be measured empirically, which limits the model's applicability. Finally, Wethey reports on the results of a heat-budget model for the surface temperature of intertidal rocks (from which he infers the temperature of acorn barnacles) (Wethey, 2002), but the details of the model itself are not divulged and the model's prediction of maximum temperature on some days differ from co-occurring measured values by more than 6K.

The heat-budget models of Bell and Helmuth serve as a useful basis for future studies: Bell's model for *M. papillatus* can easily be adjusted to provide estimates for other algae, and Helmuth's model for *M. californianus* can be adjusted for use with other mussels. There are, however, many intertidal organisms for which these two models do not suffice. For instance, limpets attach to the rock by a large foot. As a result, they have substantial conductive contact with the substratum and require a model substantively different from that of Bell or Helmuth.

The goal of this report is to describe and verify a simple heat-budget model for *Lottia gigantea* Sowerby, a common intertidal limpet of the California coast. This model can then serve as a prototype for other intertidal species with conductance-mediated temperatures, such as keyhole limpets, barnacles, chitons, abalones, certain snails, and encrusting plants and animals. Use of this model is detailed in a companion article (Denny et al., 2006).

Materials and methods

The heat budget equation

The fundamental theory underlying heat-budget models is described in detail elsewhere (Gates, 1980; Campbell and Norman, 1998; Nobel, 1999); only the condensed results of theory are presented here.

Because energy is conserved, the difference between the rate at which heat energy enters an organism (W_{in}, measured in W) and the rate at which energy leaves (W_{out}) must equal the rate at which energy is stored within the organism (W_{stored}). If we use a convention in which heat transfer into an organism is added and heat transfer out is subtracted, the conservation of heat energy can be written as:

$$W_{in} - W_{out} = W_{stored} . \quad (1)$$

For a limpet, the rates of energy transfer into and out of the organism have several components (Fig. 1):

$$W_{sw} \pm W_{lw} \pm W_{cd} \pm W_{cv} \pm W_e + W_m = W_{stored} . \quad (2)$$

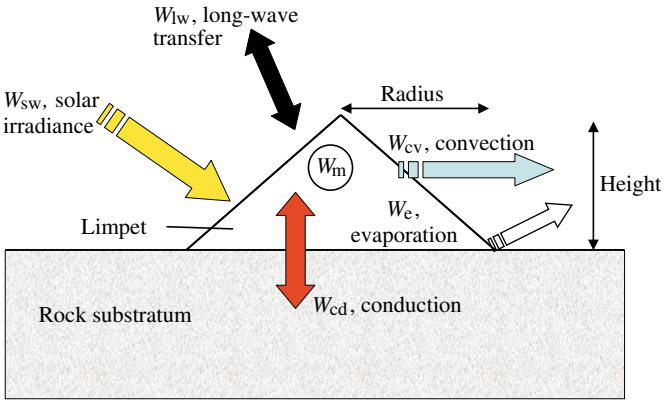

Fig. 1. A schematic representation of heat transfer to and from a limpet. Dimensions of the model limpet (its radius and height) are shown.

Here, W_{sw} is the rate of heat absorbed from short-wave (= solar) radiation (wavelength <1200 nm), and W_{lw} is the net heat transferred by long-wave (= infrared) radiation (wavelength >4000 nm). W_{cd} is the rate of heat transfer by conduction to the substratum, W_{cv} is the rate of heat transfer by convection to the air, and W_e is the rate of heat transfer by evaporation or condensation. W_m is the rate of heat production by metabolism.

This equation can be simplified by canceling out terms that are negligible. For example, the metabolic rate of limpets is low, so heat produced by metabolism can safely be neglected. Similarly, the small thermal mass of limpets and their intimate contact with both air and rock ensure that heat storage is negligible, and W_{stored} is set to zero. By doing so, we essentially assume that the organism is always at thermal equilibrium with its surroundings. Finally, for present purposes we assume that the limpet has its shell firmly clamped against the substratum, thereby preventing evaporation, and we ignore any effects of condensation. Thus, W_e=0. (Note, this may not hold for other species.) We are then left with a simplified approximation to the equation for energy conservation:

$$W_{sw} \pm W_{lw} \pm W_{cd} \pm W_{cv} = 0 . \quad (3)$$

Each of these heat fluxes can be described as a function of measurable aspects of the environment and of body temperature. The equation can then be solved to predict body temperature as a function of the thermal environment.

The components of heat flux

Short-wave heat transfer

The rate at which heat is absorbed from solar radiation is:

$$W_{sw} = A_p \alpha_{sw} I_{sw} = q_1 , \quad (4)$$

where A_p is the area of the limpet's shell (m^2) projected in the direction at which sunlight strikes the organism, α_{sw} is the short-wave absorptivity of the shell (the fraction of light energy that is absorbed), and I_{sw} is the solar irradiance (W m^{-2}). As noted in Eqn 4, this expression for absorbed energy can be

expressed as a single coefficient, q_1, for eventual use in the calculation of body temperature.

Long-wave energy transfer

According to the Sefan–Boltzmann relationship (Gates, 1980), a body at absolute temperature T emits radiation at a rate E_{lw} (W m^{-2}):

$$E_{lw} = \epsilon_{lw}\sigma T^4 , \quad (5)$$

where ϵ_{lw} is the long-wave emissivity of the object and σ is the Stefan–Boltzmann constant (5.67×10^{-8} W m^{-2} K^{-4}). As a consequence, long-wave radiation impinges on the lateral area of a limpet shell (A_l) from its environment, and the shell emits radiation to its surroundings (Fig. 1). The difference between these two fluxes determines the net radiative heat transfer.

Because the limpet and objects in its immediate vicinity (e.g. the rock) are at nearly the same temperature and have nearly the same emissivity, there is little net radiative exchange of heat between them; the effective radiative transfer of heat is between the shell and the sky. This exchange occurs over the fraction of A_l that 'sees' the sky, a fraction known as the view factor, V_s (see Campbell and Norman, 1998). If we assume that the temperature of the shell is equal to the limpet's body temperature, T_b, the total effective rate at which energy is radiated from limpet to sky is:

$$W_{lw,s} = V_s A_l \epsilon_{lw,s}\sigma T_b^4 , \quad (6)$$

where $\epsilon_{lw,s}$ is the long-wave emissivity of the shell. Similarly, the rate at which long-wave radiation from the sky is absorbed by the shell is:

$$W_{lw,a} = V_s A_l \alpha_{lw,s}\epsilon_{lw,a}\sigma T_a^4 . \quad (7)$$

Here $\alpha_{lw,s}$ is the long-wave absorptivity of the shell, and $\epsilon_{lw,a}$ and T_a are the effective long-wave emissivity and local temperature of the air, respectively.

The ability of an object to emit light at a certain wavelength is equal to its ability to absorb at that wavelength (Nobel, 1999). Substituting $\epsilon_{lw,s}$ for $\alpha_{lw,s}$ and subtracting the heat radiated from the heat absorbed, we calculate the net rate of long-wave energy transfer:

$$W_{lw} = W_{lw,a} - W_{lw,s} = V_s A_l \epsilon_{lw,s}\epsilon_{lw,a}\sigma T_a^4 - V_s A_l \epsilon_{lw,s}\sigma T_b^4 ,$$

$$W_{lw} = V_s A_l \epsilon_{lw,s}\sigma(\epsilon_{lw,a}\sigma T_a^4 - T_b^4) . \quad (8)$$

For simplicity in solving for body temperature, this expression can be linearized utilizing a Taylor expansion around T_a:

$$W_{lw} \cong V_s A_l \epsilon_{lw,s}\sigma T_a^4(\epsilon_{lw,a}-1) + 4V_s A_l \epsilon_{lw,s}\sigma T_a^3(T_a - T_b) = q_2 + q_3(T_a - T_b) . \quad (9)$$

Convective heat transfer

The rate at which a limpet gains or loses heat convectively is governed by Newton's law of cooling:

$$W_{cv} = h_c A_{cv}(T_a - T_b) = q_4(T_a - T_b) . \quad (10)$$

Here A_{cv} is the area of the shell in convective contact with the air; we assume that $A_{cv}=A_l$. The convective heat transfer coefficient (h_c, W m^{-2} K^{-1}) is an empirically measured function of the shape and size of the shell and of the local wind speed.

Conductive heat transfer

Contact of the limpet's foot with the rock substratum allows heat to be transferred diffusively between the two at a rate

$$W_{cd} = A_{cd}K_r\left(\frac{dT_r}{dz}\right) . \quad (11)$$

A_{cd} is the area of conductive contact between the limpet's foot and the rock, and K_r is the conductivity of the rock (W m^{-1} K^{-1}). T_r is the temperature of the rock as a function of distance z (m) below the surface, with z is measured as positive going into the rock. Note that it is the temperature gradient in the rock, rather than that in the limpet, that is assumed to control the rate of heat transfer. It is likely that circulation (rather than diffusion) is the primary transporter of heat within the limpet's body, and thus it is the diffusion of heat in the rock that governs the rate of transfer.

The gradient of temperature in the rock is estimated from the one-dimensional heat equation (Incropera and DeWitt, 2002):

$$\frac{\partial T_r}{\partial t} = k\left(\frac{\partial^2 T_r}{\partial z^2}\right) . \quad (12)$$

Here, t is time (s) and k is the thermal diffusivity of the rock (m^2 s^{-1}).

A simple finite-difference approach is used to solve Eqn 12. Temperature in the rock is calculated at a series of nodes. Node 1 is at the rock's surface (immediately under the limpet's foot). Node 2, is a distance Δz into the rock; node 3, $2\Delta z$ in; and so on to node n+1. The calculation begins with node 1 set to the body temperature of the limpet; that is $T_1=T_b$. Initially, all other nodes are set to ocean temperature. The first spatial derivative of temperature is then estimated for positions intermediate between each pair of nodes:

$$\left(\frac{\partial T_r}{\partial z}\right)_i \cong \frac{T_i - T_{i-1}}{\Delta z} , \qquad i = 2 \ldots n \quad (13)$$

and the second derivative is estimated at the nodes:

$$\left(\frac{\partial^2 T_r}{\partial z^2}\right)_i \cong \frac{\left(\frac{\partial T_r}{\partial z}\right)_i - \left(\frac{\partial T_r}{\partial z}\right)_{i-1}}{\Delta z} , \qquad i = 2 \ldots n . \quad (14)$$

The new temperature at each node is then calculated according to Eqn 12 as:

$$T_{i,new} = T_{i,old} + k\left(\frac{\partial^2 T_r}{\partial t^2}\right)_i \Delta t , \qquad i = 2 \ldots n . \quad (15)$$

At this point in the calculation, the body temperature of the limpet (which controls the temperature at node 1) and the new rock temperature at node 2 (a distance Δz into the rock) are known, allowing us to estimate the temperature gradient at the surface:

$$\frac{\partial T_r}{\partial z} \cong \frac{T_2 - T_b}{\Delta z} . \quad (16)$$

Conductive heat flux into or out of the limpet is then calculated per Eqn 11:

$$W_{cd} = A_{cd}K_r \frac{dT_r}{dz} \cong \frac{A_{cd}K_r}{\Delta z} (T_2 - T_b) = q_5(T_2 - T_b) . \quad (17)$$

A time step of 30 s and a spatial increment of 1 cm were used in our model (conditions under which this finite difference solution is stable), and n=200, such that the calculation is carried out to a depth of z=2 m (approximately equal to the tidal range at the experimental site). Because the spatial variation in rock temperature is not known initially, some time is required for this numerical solution to 'relax' into a realistic estimate. The time required can be estimated by calculating the time t_r it takes for a thermal signal at the rock's surface to reach the level in the rock maintained at sea-surface temperature (z=2 m):

$$t_r \cong \frac{z^2}{4\pi k} \quad (18)$$

[(Carslaw and Jaeger, 1959), p. 66].

For the thermal conductivity of granite at Hopkins Marine Station (1.49×10^{-6} m^2 s^{-1}), t is 2.5 days, and we allow 3 days for complete relaxation.

Solving for body temperature

Having in hand the expressions for the various fluxes of heat, we can now solve for body temperature. Inserting each flux equation (Eqn 4, 9, 10 and 17) into Eqn 3, we see that:

$$q_1 + q_2 + q_3(T_a - T_b) + q_4(T_a - T_b) + q_5(T_2 - T_b) = 0 ,$$

$$\therefore T_b = \frac{q_1 + q_2 + (q_3+q_4)T_a + q_5T_2}{q_3 + q_4 + q_5} . \quad (19)$$

Note that all coefficients on the right-hand side of this equation depend solely on measured constants regarding the size, shape and materials of the system, or on measurable meteorological variables.

Measuring the parameters of the model

General

The limpet is modeled as a cone of radius R and height H (Fig. 1). Thus,

$$A_{cd} = \pi R^2 , \quad (20)$$

$$A_1 = \pi R \sqrt{H^2 + R^2} . \quad (21)$$

A_p, the projected area of the cone, is calculated as a function of the instantaneous direction of sunlight relative to the orientation of the shell (Pennell and Deignan, 1989).

Short-wave flux (Eqn 4)

Absorptivity, α_{sw}, was measured for four dry shells of *L. gigantea.* A spectroradiometer (model 1800 equipped with an intergrating sphere, Li-Cor Inc., Lincoln, NE, USA) was used to measure the absorbance of the shell at wavelengths between 300 and 1100 nm; values were averaged among the four shells. Each average wavelength-specific absorbance was then weighted by the fraction of overall solar irradiance at that wavelength and summed across wavelengths to provide the effective α_{sw} for the shell. Solar irradiance, I_{sw}, is one of the meteorological inputs into the model, and is quantified using a pyranometer. This instrument measures the solar energy (per square meter) falling on a horizontal surface, and with knowledge of the path of the sun across the sky can be used to calculate I_{sw}, the rate at which energy falls on a surface held perpendicular to the direction of incoming sunlight. The path of the sun on any given day is calculated from the local latitude, longitude, and time using relationships described in detail elsewhere (Gates, 1980).

Long-wave flux (Eqn 9)

The average long-wave emissivity of two *L. gigantea* shells ($\epsilon_{lw,s}$) was measured using an IR Snapshot model 525 infrared camera (Infrared Solutions, Inc., Minneapolis, MN, USA). For a clear sky, the long-wave emissivity of air, $\epsilon_{lw,a}$, is approximately $9.2\times10^{-7}T_a^2$ (Campbell and Norman, 1998); for a cloudy sky, $\epsilon_{lw,a}$ is approximately 1. T_a is a meteorological input into the model. The view factor, V_s, for a given spot on the substratum is measured by placing a camera equipped with a 'fish-eye' lens at that spot, and taking a picture directed perpendicularly away from the rock. The fraction of the picture that is sky is the view factor.

Convective heat flux (Eqn 10)

The convective heat transfer coefficient, h_c, of three *L. gigantea* shells was measured as follows. A thermocouple was inserted into the base of a silver-alloy cast of each shell and the shells were placed on a non-conducting substratum (a Styrofoam block) on the floor of a wind tunnel. Silver was used because its high thermal conductivity ensures that the temperature of the cast is virtually constant throughout, allowing a single thermocouple to measure 'the' temperature of the object, T_b. A series of plaster-of-Paris plates (each cast with the surface texture of granite) were aligned upstream of the limpets over a distance of 1 m to ensure that the boundary-layer air flow around the limpets was similar to that encountered in the field. A model 441S thermistor anemometer (Kurz, Inc., Monterey, CA, USA) measured the wind speed 25 cm above the limpets, and a thermocouple measured the air temperature, T_a. Each model was heated to 30K above air temperature and the time course of its cooling was recorded by a CR21X datalogger (Campbell Scientific, Inc., Logan, UT,

USA). The experiment was repeated for a series of wind speeds ranging from 0.25 to 5.10 m s^{-1} at each of three shell orientations (anterior upstream, downstream, and at right angles to the wind). The convective area of each shell, A_c, was measured by carefully coating the exposed area of the shell with aluminum foil, and weighing the foil. The mass, m, of each cast was measured, and the specific heat of the silver alloy, c_{Ag}, is 235 J kg^{-1} K^{-1}. If the logarithm of T_b–T_a is plotted as a function of time (s), the slope of the line is:

$$\text{Slope} = -\frac{h_c A_c}{m c_{Ag}} , \quad (22)$$

from which h_c can be calculated. Measured heat transfer coefficients were corrected for the slight loss of heat to the Styrofoam substratum.

Variation in h_c with wind speed and size of shell is traditionally expressed as the variation in the Nusselt number (Nu) as a function of the Reynolds number (Re), where:

$$Nu = \frac{2h_c R}{K_a} , \quad (23)$$

$$Re = \frac{2uR}{\nu} . \quad (24)$$

Here K_a is the conductivity of air (W m^{-1} K^{-1}), u is the wind speed (m s^{-1}), and ν is the kinematic viscosity of air (m^2 s^{-1});

$$K_a \cong 0.00501 + 7.2 \times 10^{-5} T_a , \quad (25)$$

$$\nu \cong -1.25 \times 10^{-5} + 9.2 \times 10^{-8} T_a , \quad (26)$$

[relationships calculated from data presented previously (Denny, 1993)]. Typically, the functional relationship between Nu and Re can be expressed in the form:

$$Nu = aRe^b . \quad (27)$$

The coefficients a and b can be estimated from a linear regression of logNu *versus* logRe (Table 1), and in turn can be used to estimate h_c for a limpet of any realistic size encountering any given wind speed:

$$h_c \cong a \left(\frac{K_a u}{\nu} \right)^b R^{b-1} . \quad (28)$$

The r^2 values were >0.99 in the regression for each object and orientation. Values for shells broadside to the wind were used in the model.

Conductive heat flux

The thermal diffusivity of the rock is related to its thermal conductivity:

$$k = \frac{K_r}{\rho c_r} , \quad (29)$$

where ρ is the mass density of the rock and c_r is its specific heat capacity (Carslaw and Jaeger, 1959).

Values of all parameters used in the model are shown in Table 1, and a list of symbols is provided in Table 2. Our model could be applied to other species by using the appropriate species-specific values for these parameters.

Testing the heat-budget model

The results from the heat-budget model were compared to temperatures measured in the field for three types of objects: (1) a silver-alloy cone, (2) an actual *L. gigantea* shell enclosing a silver-alloy body, and (3) two live *L. gigantea*.

A cone was chosen as the first test of the model because this is the shape with which the model approximates a limpet. The cone (whose surface was black from the casting process) was

Table 1. *Values for parameters used in the heat-budget model*

Parameter	Units	Cone	Silver-bodied limpet	Live limpet
α_{sw}	None	0.86	0.68	0.68
α_{lw}	None	0.90	0.97	0.97
$\epsilon_{lw,s}$	None	0.90	0.97	0.97
V_s	None	0.7	0.7	0.7
R	cm	1.83	1.76	2.23
H	cm	1.83	1.22	1.10
K_r	W m^{-1} K^{-1}	3.06	3.06	3.06
ρ	kg m^{-3}	2601	2601	2601
c_r	J kg^{-1} K^{-1}	789	789	789
k	m^2 s^{-1}	1.49×10^{-6}	1.49×10^{-6}	1.49×10^{-6}
a (anterior upwind)	None	1.660	1.955	1.955
b (anterior upwind)	None	0.389	0.371	0.371
a (posterior upwind)	None		1.881	1.881
b (posterior upwind)	None		0.376	0.376
a (broadside)	None		1.304	1.304
b (broadside)	None		0.404	0.404

a and b are the coefficients for the Nusselt–Reynolds number relationship (Eqn 27).

Table 2. *Symbols used in the text and the equation in which each is introduced*

Symbol	Definition	Units	Equation
a	*Nu–Re* coefficient	None	27
A_{cd}	Conductive area	m^2	11
A_{cv}	Convective area	m^2	10
A_l	Lateral area	m^2	6
A_p	Projected area	m^2	4
b	*Nu–Re* exponent	None	27
c_{Ag}	Specific heat of silver	J kg^{-1} K^{-1}	22
c_r	Specific heat of rock	J kg^{-1} K^{-1}	29
E_{lw}	Rate of energy emission	W m^{-2}	5
H	Height of shell	m	21
h_c	Heat transfer coefficient	W m^{-2} K^{-1}	10
i	Node number (i=1 at surface)	none	13
I_{sw}	Solar irradiance	W m^{-2}	4
K_a	Thermal conductivity of air	W m^{-1} K^{-1}	23
K_r	Thermal conductivity of rock	W m^{-1} K^{-1}	11
k	Thermal diffusivity of rock	m^2 s^{-1}	12
m	Mass	kg	22
n	Number of nodes	None	13
Nu	Nusselt number	None	23
q_1	Coefficient	W	4
q_2, q_3	Coefficients	W, W K^{-1}	9
q_4	Coefficient	W K^{-1}	10
q_5	Coefficient	W K^{-1}	17
R	Radius of shell	m	20
Re	Reynolds number	None	24
t	Time	s	12
T	Temperature	K	5
T_a	Air temperature	K	7
T_b	Body temperature	K	6
T_i	Temperature at node i	None	13
T_r	Rock temperature	K	11
u	Wind speed	m s^{-1}	24
V_s	View factor	None	7
W_{cd}	Conductive heat transfer rate	W	2
W_{cv}	Convective heat transfer rate	W	2
W_e	Evaporative heat transfer rate	W	2
W_{in}	Inward heat transfer rate	W	1
W_{lw}	Long-wave heat transfer rate	W	2
$W_{lw,a}$	Long-wave heat transfer rate from air	W	7
$W_{lw,s}$	Long-wave heat transfer rate to air	W	6
W_m	Metabolic heat transfer rate	W	2
W_{out}	Heat transfer rate out	W	1
W_{sw}	Short-wave heat transfer rate	W	2
z	Distance into rock	m	11
α_{sw}	Short-wave absorptivity	None	4
$\alpha_{lw,s}$	Long-wave absorptivity of shell	None	7
ϵ_{lw}	Long-wave emissivity	None	5
$\epsilon_{lw,a}$	Long-wave emissivity of air	None	7
$\epsilon_{lw,s}$	Long-wave emissivity of shell	None	6
ν	Kinematic viscosity of air	m^2 s^{-1}	24
ρ	Density of rock	kg m^{-3}	29
σ	Stefan–Boltzmann constant	Wm^{-2} K^{-4}	5

placed on a horizontal granite surface just above the intertidal zone at Hopkins Marine Station, Pacific Grove, CA, USA (36.67°N, 121.88°W). A thin layer of heat-conductive paste (Wakefield 120-8 thermal compound, Wakefield Engineering, Wakefield, MA, USA) between the base of the cone and the substratum ensured good thermal contact. Solar irradiance was measured using a LI-200SB pyranometer (Li-Cor, Inc., Lincoln, NE, USA) located approximately 1.5 m from the cone. Wind speed 25 cm above the substratum was measured using a Wind Sentry cup anemometer (R. M. Young Co., Traverse City, MI, USA) located approximately 1.5 m from the cone. Rock temperature was measured by scraping a shallow (approx. 1 mm deep) groove in the rock adjacent to the cone, attaching a fine thermocouple (40 gauge wire) to the groove with thermally conducting paste, and sprinkling granite dust over the groove. Shaded air temperature was measured with a thermocouple 10 cm above the substratum, located approximately 25 cm from the cone. All variables were recorded every 30 s using a CR21X datalogger (Campbell Scientific, Logan, UT, USA). The view factor of the cone was estimated as described above.

Measurements were made continuously from 12 to 20 September, 2003. These days were characterized by clear skies and had among the highest air temperatures of the year. Several nights during the experiment were foggy, and the effective long-wave emissivity of the sky was set at 1.0 for those periods.

The silver-bodied limpet was tested at the same time (and in the same fashion) as the cone. To form this physical model, a representative *L. gigantea* shell was filled with wax, and the wax was removed. The wax 'body' was then cast in silver and reunited with its shell. A thin layer of heat-conductive paste between the silver body and the inside of the shell ensured good conduction of heat from shell to body. This physical model serves as an intermediate between the cone (an abstract limpet) and a live limpet. The silver-bodied limpet has an actual shell, but it can neither move nor evaporate water, thereby avoiding potential complicating factors inherent with live animals.

Two live *L. gigantea* were tested in the same manner as the cones and silver-bodied limpets (and at the same site) on 18 and 19 October, 2003. Animals were gently dislodged from the rocks at Hopkins Marine Station and placed at the experimental site. To measure body temperature, a 40-gauge thermocouple was sandwiched between the foot and the substratum.

For each experiment, the recorded meteorological data and the known physical characteristics of each test object and the rock were used in the heat-budget model to predict the time course of body temperature. These temperatures could then be compared to actual, recorded body temperatures. As noted above, for experiments with the cone and the silver-bodied limpet, data for the first 3 days of the experiment were used to allow the model to relax into independence from its starting conditions, and the last 5 days were used to compare the model to the measured cone temperatures. It was not possible to leave the live limpets exposed for longer than a day, so an alternative

method was used to bring the numerical model of rock temperature up to speed. The model was initiated as described above, and the results at the end of the day were then used as the starting condition for a repetition of the calculation. This procedure was repeated three times, and the third repetition was used as the final estimate.

Sensitivity analyses

Sensitivity of predicted body temperature to changes in selected input parameters was tested by varying each parameter separately by ±10% while all other parameters were kept at their standard values, as listed in Table 1. For each test, the model was run using 5 years of measured environmental data (Denny et al., 2006) and the change in overall maximum predicted body temperature was noted, measured relative to the temperature obtained with standard values. The limpet was assumed to lie on a horizontal surface 1.5 m above mean lower low water, the position that results in the highest body temperature (see Denny et al., 2006). The parameters chosen for analysis are those related to radiative heat transfer (α_{sw}, $\epsilon_{lw,s}$), topography (the view factor, V_s), the conductive characteristics of the rock (thermal diffusivity, k, and thermal conductivity, K_r), and the convective characteristics of the shell (the coefficients a and b for the *Nu–Re* relationship, Eqn 27). Analysis of the sensitivity of predicted body temperature to other parameters (wind speed, solar irradiance, air temperature, angle of the substratum, etc.) amounts to an exploration of how the model functions in the presence of real-world variability, and is discussed in the accompanying paper (Denny et al., 2006).

We note that the coefficients for the *Nu–Re* relationship are not independent values. Tests on a variety of shapes (sphere, hemisphere, cone, and cylinders of two aspect ratios) showed that an increase in a is correlated with a decrease in b (r^2=0.82, N=5, P=0.0345). The slope of this relationship is such that a 10% increase in a is accompanied by a 4.96% decrease in b, and this relationship has been used in our sensitivity analysis. The ±10% variation in thermal conductivity used in this analysis incorporates a ±10% change in either the density of the rock or its specific heat capacity. Consequently, variation in density and heat capacity are not tested separately.

Results

Cone

The time course of temperature (both predicted and actual) is shown in Fig. 2 for the experimental cone. The model tended to underestimate 'body' temperature slightly during the night, but daytime temperatures (especially near-maximal temperatures) were modeled accurately. This presentation of the data can be misleading, however, for those periods when temperature changes rapidly. To circumvent this problem, the same data are replotted in Fig. 3, which makes it more evident how the data cluster around the line of equality between prediction and measurement. The model predicted temperatures that rose faster in the morning and fell faster in the evening than those actually measured, leading to the loop-like appearance of the data. The measured temperature was, on average, 1.25K above the predicted value, and the standard deviation of the deviations from the predicted temperature (the root-mean-square average) was 1.31K. For the highest 5% of predicted temperatures (those that might be most dangerous to a limpet), the measured temperature was, on average, different from the predicted temperature by only –0.02K, with a standard deviation of this deviation equalling 0.48K.

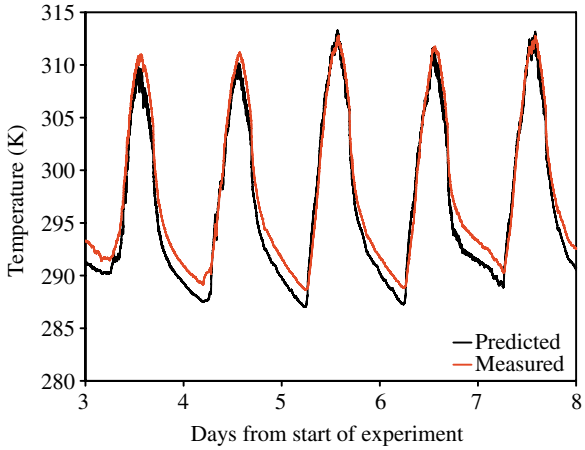

Fig. 2. The time series of measured (red line) and predicted (black line) body temperatures for the silver cone. The time series starts at day 4 of the experiment, allowing time for equilibration of estimated rock temperatures. The heat-budget model slightly underestimates body temperatures at night, but accurately predicts maximal temperatures during the day.

Silver-bodied limpet

The temporal data for the silver-bodied limpet were very similar to those for the cone, and the plot of predicted *versus*

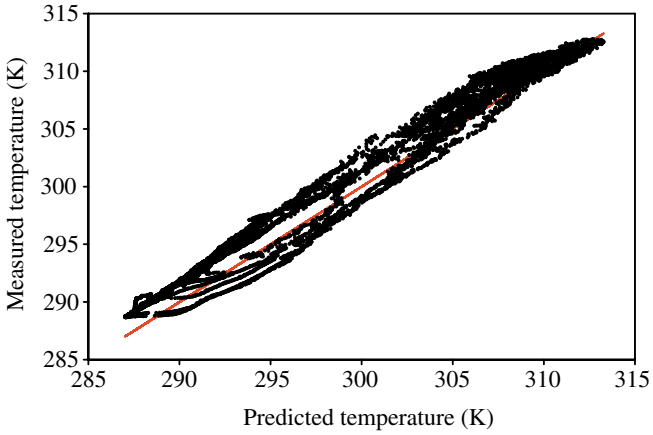

Fig. 3. The data from Fig. 2 replotted to emphasize deviations between predicted and measured temperatures for the silver cone. The line of equivalence between predicted and measured temperature is shown in red.

measured values is shown in Fig. 4. In this case, the measured temperature was 0.39K below the predicted value (on average), and the standard deviation of temperature deviations was 1.19K. Again, the model performed quite well at predicting the highest temperatures of the test object. For the highest 5% of predicted temperatures, the measured temperature was 0.51K below the predicted temperature, with a standard deviation of 0.47K.

Live limpets

The data for live limpets are shown in Fig. 5. In one case (Fig. 5A), the model predicted the limpet's body temperature within 0.55K on average (s.d.=0.91K). In the second case (Fig. 5B), the model predicted the limpet's temperature within –0.05K on average (s.d.=0.62K). Predictions were even closer when body temperature was highest. For the highest 5% of predicted temperatures, the average difference between measurement and prediction was 0.29K for the first limpet and –0.09K for the second limpet (s.d.=0.26K and 0.25K, respectively).

Heat-flux components

Measurements from a typical day are shown in Fig. 6, comparing limpet body temperature, rock temperature and air temperature. Both body and rock temperatures were consistently higher than air temperature. In contrast, body temperature was typically within a degree of rock temperature. The slight temporal disparity between rock temperature and body temperature in the late afternoon (circled in Fig. 6) was due to the spatial separation between the sites of the two measurements. The site of the rock measurement entered the shadow of the setting sun before the limpet.

The various fluxes contributing to body temperature are shown in Fig. 7 for the day shown in Fig. 6. During the middle of the day (when body temperature is highest), solar irradiance is the largest source of heat influx to the limpet, whereas convection and conduction are of similar magnitude in transporting heat out of the limpet. After the sun has set, conduction of heat from the rock becomes the largest influx to the limpet. It is this conductive heat transfer that maintains the limpet at a temperature several degrees above air temperature throughout the night.

Prior to dawn on the day shown in Fig. 7, the sky was foggy, whereas after dusk, the sky was clear. The larger long-wave flux is evident in the latter case.

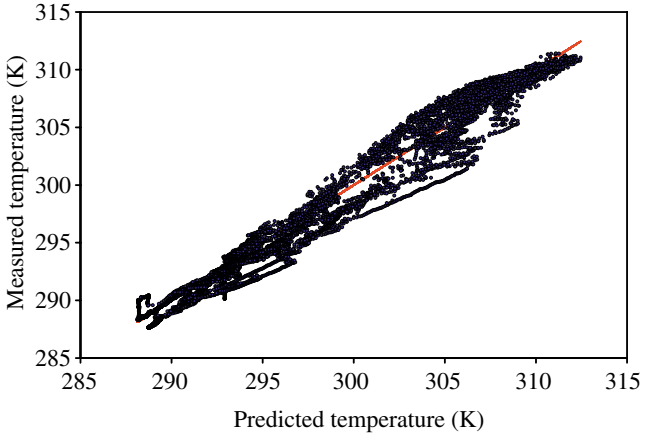

Fig. 4. Predicted and measured temperatures for the silver-bodied limpet. There are deviations between prediction and measurement at moderate temperatures, but close agreement at high temperatures. The line of equivalence between predicted and measured temperature is shown in red.

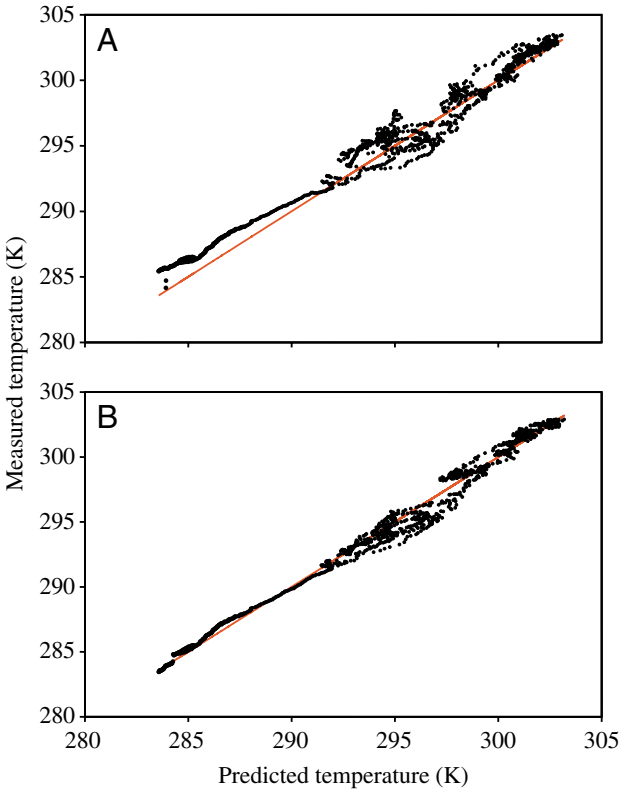

Fig. 5. Predicted and measured temperatures for live limpets. The line of equivalence between predicted and measured temperature is shown in red. A and B show the results of two separate experiments on two different limpets.

Sensitivity analyses

A 10% change in parameter values had only minor effect on predicted maximum body temperature (Table 3). The largest effect was for a change in short-wave absorptivity, where a ±10% variation yielded a change of approximately ±1.25K in 5-year maximum body temperature.

Discussion

Applications of the model

Our simple heat-budget model predicts the body temperature of limpets and limpet-like physical models with notable

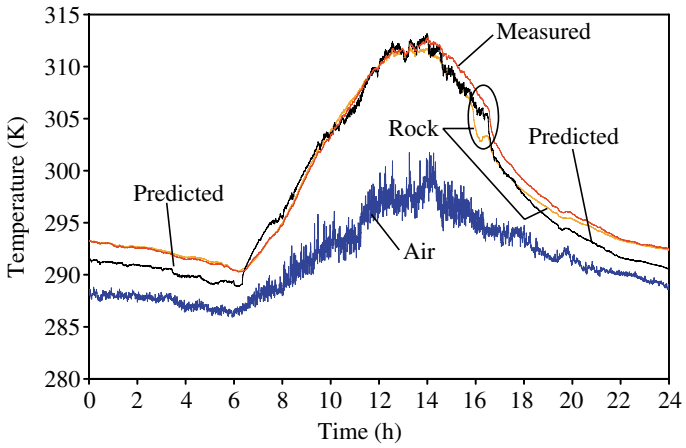

Fig. 6. Rock temperature, as well as both measured and predicted limpet body temperatures, exceed air temperature throughout a typical day. The circled deviation between rock and body temperatures is due to spatial separation between locations of the two measurements: the rock entered the shadow of the setting sun prior to the limpet.

Table 3. *Change in 5-year maximum body temperature for a ±10% change in a given parameter used in the heat-budget model*

Parameter	Change in maximum body temperature (K)	
	+10%	–10%
α_{sw}	+1.30	–1.26
$\epsilon_{lw,s}$	–0.07*	+0.21
V_s	–0.21	+0.21
K_r	–0.62	+0.65
k	–0.32	+0.34
a (broadside)†	+0.27	–0.22

a and b are the coefficients for the Nusselt–Reynolds number relationship (Eqn 27).

*The standard long-wave emissivity, 0.97, is increased to the maximum possible value, 1.0, for this calculation.

†As explained in the text, an increase of 10% in a is accompanied by a decrease of 4.96% in b.

accuracy on days conducive to exceptionally high body temperatures, suggesting that the model may be of practical use in exploring the thermal biology of organisms whose temperatures are strongly affected by conductive heat transfer to and from the substratum. For example, as a convenient means of translating meteorological data into time-, site- and species-specific body temperatures, the model we present here provides a means to examine:

(1) The importance of small-scale and short-term variability

In the intertidal zone, temperatures vary drastically through time and space, and heat-budget models allow us to explore this variability with spatial and temporal resolution that would be daunting to achieve with direct field measurements. For example, the model allows one to compare body temperatures among individuals of different morphology at any given site, or among individuals of constant morphology at sites of different topography.

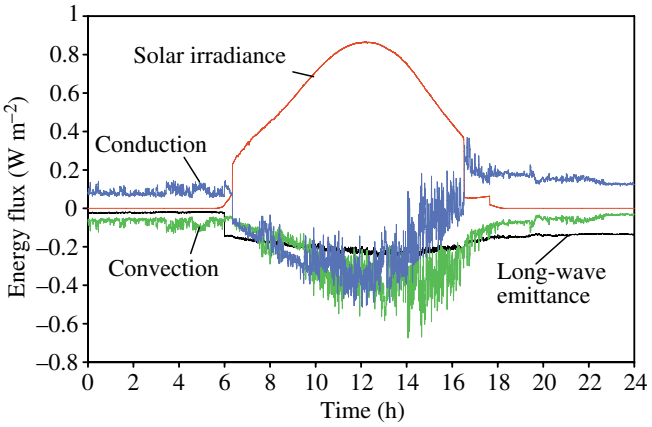

Fig. 7. Heat fluxes for the day shown in Fig. 6. Near midday, when limpet temperature is highest, heat is shed by convection (green line) and conduction (blue line) in roughly equal amounts.

(2) The frequency distribution of stressful events through time

The thermal stress imposed on organisms depends both on maximum body temperature and the time course and duration of temperatures leading up to that maximum. When coupled with meteorological records, heat-budget models can provide lengthy time series of body temperatures to aid physiologists in designing appropriate regimes for testing the effects of thermal stress.

(3) The effectiveness of morphological and behavioral adaptations

Do the ribs on certain limpet shells act as cooling fins? Does the 'mushrooming' behavior of some limpets (in which the shell is lifted free of the substratum) allow effective evaporative cooling? Is variation in shell color a viable adaptive strategy in coping with thermal stress? Adjustment of parameters within the heat-budget model allows one to predict the magnitude of these effects.

(4) The biological implications of future climate scenarios

How would a 4K increase in air temperature affect limpet body temperature? The heat-budget model provides a ready answer.

Aspects of topics 1 and 2 are addressed in the accompanying paper (Denny et al., 2006), and ongoing research is beginning to address topics 3 and 4 (C. D. G. Harley and K. Mach, unpublished data). In future research, our model can be used in conjunction with the earlier ones (Bell, 1995; Helmuth, 1998) to predict the temperature of many ecologically species important in intertidal community structure, and thereby to provide a valuable physiological perspective on intertidal community ecology.

Limitations of the model

Several limitations on the model should be recognized, however. First, the model is constrained by the simple, one-dimensional calculation of conductive heat flux. In our experiments, both the short-wave absorptivity of the rock (0.57) and its convective heat transfer coefficient (Nu=0.618$Re^{0.477}$) were slightly below those of the limpet. As a consequence, during the day the rock near the limpet absorbed less heat from the sun, but also lost less heat to convection, with the net result that the rock temperature was very close to that of the limpet. Thus, during the day, there was likely very little lateral temperature gradient in the rock surrounding the limpet, and the model's assumed one-dimensional gradient of rock temperature was therefore accurate. At night, however, when neither rock nor limpet had any solar heat influx, the difference in convective heat transfer coefficient becomes evident. Because the rock has a lower h_c than the limpet, it cools more slowly. The relatively warm rock surrounding the base of the relatively cool limpet in reality leads to a radial flow of heat into the limpet. In the model, however, this lateral heat transfer is not allowed, with the result that the model predicts a temperature slightly lower than that actually measured. An appropriate three-dimensional model can be constructed (see Incropera and DeWitt, 2002), but it will be more computationally intense.

The requirement in the current model that conductive heat transfer in the rock be essentially one-dimensional places some practical constraints on the disparity in absorptivities that can be accommodated between the rock and the limpet. A highly reflective limpet on a highly absorptive rock (or *vice versa*) could lead to substantial lateral transfer of heat, thereby degrading the accuracy of the model. Evolution appears to have mediated against this scenario, however. The color (and, presumably, the absorptivity) of most limpets is reasonably similar to the rock on which they are found, perhaps as a means of avoiding visual predation.

The model (which does not take into account evaporative cooling) accurately predicted the temperatures of both silver-bodied and live limpets. If, in reality, the live limpet had been substantially affected by evaporative cooling, the model would have overestimated its temperature. It seems likely, then, that evaporation did not play an important role in the heat budget of the two live limpets used in this experiment. This does not rule out the potential importance of evaporative cooling under other circumstances and for other species, and this factor requires further research.

Convective heat transfer coefficients typically increase roughly in proportion to the square root of wind speed (Bird et al., 1960), and the values for limpets are no exception (Table 1). As a consequence, convective heat flux is very sensitive to the lowest range of wind speeds: for example, a slight breeze too slow to be measured by a cup anemometer (<0.2 m s^{-1}) might nonetheless have a substantial cooling effect on a limpet. Consequently, care must be taken when applying our model to low-speed wind conditions using standard cup anemometers lest body temperature be overestimated. For example, because rock and limpet temperatures are typically higher than those of the surrounding air, slow free convection will commonly be present even when a cup anemometer indicates no flow. Only in unusual microhabitats is the flow ever likely to be less than 0.2 m s^{-1} on a hot day.

We did not directly encounter this problem during the experiments reported here, because wind speeds during the hot part of the day never fell below 0.2 m s^{-1} for more than a few seconds at a time. The potential exists, however, for inappropriate measurements in future experiments, and care should be taken that appropriate technology (e.g. thermistor anemometers, which can measure very low wind speeds) is employed on hot, still days.

In the current model, we have assumed that the limpet is always at equilibrium with its thermal environment. The validity of this assumption was tested by constructing a non-equilibrium version of the model, and solving for body temperature explicitly as a function of time. The results were indistinguishable from those reported here. Care should nonetheless be taken when applying the model to organisms larger than those used here (e.g. to abalones).

The model is not unduly sensitive to changes in input parameters: a 10% change in any one of the tested parameter values typically results in a shift of less than 0.7K in 5-year maximum temperature. Maximum temperature is most sensitive to changes in short-wave absorptivity (±1.3K for a 10% change), and exploration of natural variation in this parameter among *L. gigantea* would be valuable.

We thank L. Hunt for insightful discussions, D. Wethey for suggesting the numerical solution to the heat equation, and D. Pantelone for his silver-casting skills. This work was funded by NSF grant OCE 9985946 to M.D. This is contribution 215 of the Partnership for Interdisciplinary Studies of the Coastal Ocean (PISCO): a Long-Term Ecological Consortium funded by the David and Lucile Packard and Gordon and Betty Moore Foundations.

References

Bell, E. C. (1995). Environmental and morphological influences on thallus temperature and desiccation of the intertidal alga *Mastocarpus papillatus* Kützing. *J. Exp. Mar. Biol. Ecol.* **191**, 29-55.

Bird, R. B., Stewart, W. E. and Lightfoot, E. N. (1960). *Transport Phenomena*. New York: John Wiley and Sons.

Campbell, G. S. and Norman, J. M. (1998). *An Introduction to Environmental Biophysics.* New York: Springer-Verlag.

Carslaw, H. S. and Jaeger, J. C. (1959). *Conduction of Heat in Solids* (2nd edn). Oxford: Clarendon Press.

Davison, I. R. and Pearson, G. A. (1996). Stress tolerance in intertidal seaweeds. *J. Phycol.* **32**, 197-211.

Denny, M. W. (1993). *Air and Water*. Princeton, NJ: Princeton University Press.

Denny, M. W., Miller, L. P. and Harley, C. D. G. (2006). Thermal stress on intertidal limpets: long-term hindcasts and lethal limits. *J. Exp. Biol.* **209**, 2420-2431.

Dethier, M. N., Williams, S. L. and Freeman, A. (2005). Seaweeds under stress: manipulated stress and herbivory affect critical life-history functions. *Ecol. Monogr.* **75**, 403-418.

Gates, D. M. (1980). *Biophysical Ecology*. Mineola, NY: Dover Publications.

Harley, C. D. G. (2003). Abiotic stress and herbivory interact to set range limits across a two-dimensional stress gradient. *Ecology* **84**, 1477-1488.

Helmuth, B. S. T. (1998). Intertidal mussel microclimates: predicting the body temperature of a sessile invertebrate. *Ecol. Monogr.* **68**, 51-74.

Helmuth, B., Kingsolver, J. G. and Carrington, E. (2005). Biophysics, physiological ecology, and climate change: does mechanism mater? *Annu. Rev. Physiol.* **67**, 177-201.

Hofmann, G. E. and Somero, G. N. (1996). Interspecific variation in thermal denaturation of proteins in congeneric mussels *Mytilus trossulus* and *M. galloprovincialis*: evidence from the heat-shock response and protein ubiquination. *Mar. Biol.* **126**, 65-75.

Incropera, F. P. and DeWitt, D. P. (2002). *Fundamentals of Heat and Mass Transfer.* New York: John Wiley and Sons.

Leonard, G. H. (2000). Latitudinal variation in species interactions: a test in the New England rocky intertidal zone. *Ecology* **81**, 1015-1030.

Newell, R. C. (1979). *Biology of Intertidal Animals*. Faversham, Kent: Marine Ecology Surveys.

Nobel, P. S. (1999). *Physicochemical and Environmental Plant Physiology* (2nd edn). New York: Academic Press.

Pennell, S. and Deignan, J. (1989). Computing the projected area of a cone. *Soc. Ind. Appl. Math. Rev.* **31**, 299-302.

Raffaelli, D. and Hawkins, S. (1996). *Intertidal Ecology*. London: Chapman & Hall.

Stillman, J. H. and Somero, G. N. (2000). A comparative analysis of the upper thermal tolerance limits of eastern Pacific porcelain crabs, Genus Petrolisthes: influences of latitude, vertical zonation, acclimation, and phylogeny. *Physiol. Biochem. Zool.* **73**, 200-208.

Tomanek, L. (2002). The heat-shock response and patterns of vertical zonation inintertidal *Tegula* congeners. *Integr. Comp. Biol.* **42**, 797-807.

Tsuchiya, M. (1983). Mass mortality in a population of the mussel *Mytilus edulis* L. caused by high temperature on rocky shores. *J. Exp. Mar. Biol. Ecol.* **66**, 101-111.

Wolcott, T. G. (1973). Physiological ecology and inertidal zonation in limpets (*Acmaea*): a critical look at 'limiting factors'. *Biol. Bull.* **145**, 389-422.

Wethey, D. S. (1984). Sun and shade mediate competition in the barnacles *Chthamalus* and *Semibalanus*: a field experiment. *Biol. Bull.* **167**, 176-185.

Wethey, D. S. (2002). Biogeography, competition, and microclimate: the barnacle *Chthmalus fragilis* in New England. *Integr. Comp. Biol.* **42**, 872-880.